Continuum limit of amorphous elastic bodies (III): Three dimensional systems

F. Léonforte, R. Boissière, Arnaud Tanguy, J.P. Wittmer, J.-L. Barrat

Continuum limit of amorphous elastic bodies (III): Three dimensional systems

F. Leonforte,[1,*] R. Boissière,[1] A. Tanguy,[1] J.P. Wittmer,[2] and J.-L. Barrat[1]

[1] *Laboratoire de Physique de la Matière Condensée et des Nanostructures, Université Claude Bernard (Lyon I) & CNRS, 43 Bvd. du 11 Nov. 1918, 69622 Villeurbanne Cedex, France*

[2] *Institut Charles Sadron, CNRS, 6, Rue Boussingault, 67083 Strasbourg, France*

Abstract

Extending recent numerical studies on two dimensional amorphous bodies, we characterize the approach of elastic continuum limit in three dimensional (weakly polydisperse) Lennard-Jones systems. While performing a systematic finite-size analysis (for two different quench protocols) we investigate the non-affine displacement field under external strain, the linear response to an external delta force and the low-frequency harmonic eigenmodes and their density distribution. Qualitatively similar behavior is found as in two dimensions. We demonstrate that the classical elasticity description breaks down below an intermediate length scale ξ, which in our system is approximately 23 molecular sizes. This length characterizes the correlations of the non-affine displacement field, the self-averaging of external noise with distance from the source and gives the lower wave length bound for the applicability of the classical eigenfrequency calculations. We trace back the "Boson-peak" of the density of eigenfrequencies (obtained from the velocity auto-correlation function) to the inhomogeneities on wave lengths smaller than ξ.

PACS numbers: 46.25.-y Static elasticity, 72.80.Ng Disordered solids, 83.70.Fn Granular solids

*Email: fleonfor@lpmcn.univ-lyon1.fr

I. INTRODUCTION.

In a recent series of papers [1, 2, 3], we investigated the elastic response of zero temperature *two* dimensional (2D) amorphous systems. Our studies were motivated by the idea that such systems, although they appear perfectly homogeneous when looking at the density field, may be described as heterogeneous from the point of view of the theory of elasticity. The basic reason for this failure is now well identified: the underlying *hypothesis of affinity* of elastic deformations, implicit in standard elastic theory, needs not to apply to a disordered system. The relevant issue is therefore the scale above which a disordered, glassy system can be considered as homogeneous from an elastic point of view.

Obviously, this question is important for the vibrational spectrum of such disordered systems; the excess of vibrational states at intermediate frequencies in the spectrum (the so called "boson peak") has previously been assigned to the existence of elastic heterogeneities [4, 5]. Moreover, the field of *plastic* deformation of glassy materials, which has attracted considerable attention recently [6, 7, 8, 9, 10, 11] may be expected to be related to elastic heterogeneities. Other points of interest include the experimental evidence for dynamical heterogeneities in deeply supercooled systems [12], which again could be expected to give rise to "frozen in" heterogeneities in low temperature systems.

Our previous studies were limited to 2D systems, as this reduced dimension allows to carry out calculations on systems with large linear sizes using a limited number of particles. These studies allowed us to establish, for a standard computational model system, the existence of a length scale that can reach a few tens of particles, and below which classical elasticity breaks down. Similar conclusions were reached by Goldenberg and Goldhirsch [13]. This breakdown is revealed by a number of different diagnostics. Firstly, the so called Born expression for elastic constants is found to give incorrect results at zero temperature (where the fluctuation term does not contribute). This failure can be traced back to the importance of a non-affine contribution to the microscopic displacement field, while the derivation of the Born formula assumes affine displacement at all scales. The analysis of the correlation function of the non-affine contribution to the displacement field reveals a length scale ξ over which this field is correlated, defining "soft" regions with large non-affine displacements. Second, the study of low frequency vibrations in these model disordered systems shows that the predictions of classical elastic theory are recovered only for wave lengths larger than ξ, meaning the

system is not homogeneous from the point of view of elastic properties below this scale. More recently, it was shown that the response to a point force is dominated by fluctuations for distances to the source smaller than ξ [3]. Hence, ξ characterises the self-averaging of the noisy response within each configuration which let us to call it the *self-averaging length*. The pressure dependence of ξ has also been investigated in 2D demonstrating that the self-averaging length remains "mesoscopic" for low and moderate pressures, typically of the order of 40 particle sizes, but decreases at large pressures [14].

An obvious question that arises is the extent to which these results may depend, qualitatively or quantitatively, on the dimensionality of space. Three dimensional (3D) systems, however, are considerably more difficult to study than the 2D case. In particular, if the elastic inhomogeneities take place on a length scale comparable to what is observed in 2D, very large systems have to be studied in order to reach the limit of elastically homogeneous systems, i.e. $L \gg \xi$ where L is the lateral size of a cubic system and ξ the size of inhomogeneities. Typical numbers of the order of at least 10^5 particles should be considered, if one wants to use the same tools and diagnostics in 2D and 3D systems. Although a number of studies have appeared recently [15, 16, 17] pointing to the existence of elastic inhomogeneities in various types of disordered systems, all of them were realised for relatively small system sizes, making a direct comparison with our previous results difficult. In the same way, previous calculations of vibration modes in 3D systems have been limited to rather small sizes [18, 19, 20]. To our knowledge, this work is the first one to explore systems with lateral sizes that are appreciably larger than the expected scale of elastic heterogeneities.

The aim of this work is therefore to characterise the elastic behavior of large 3D systems, using the same computer model and similar quench protocols as in our previous 2D studies. They are summarised in section II. In section III, we start by analysing the non-affine local displacement field in cubic samples submitted to uniaxial elastic deformation. From previous experience [1, 2], we know that this type of analysis is the most cost effective in revealing the existence of inhomogeneities and their length scale. We then discuss the elastic response to a point force (section IV) and corroborate why ξ has been termed "self-averaging length". Vibrational properties at very low eigenfrequencies – obtained by diagonalization of the dynamical matrix – are considered in section V and the density of eigenstates – computed by means of the finite temperature velocity auto-correlation function – in section VI. Our results are summarised in the last section.

II. DESCRIPTION OF SYSTEMS AND SIMULATION PROCEDURES.

The initial configurations and their preparation are very similar to those described in Ref. [1] for the 2D case. In order to make the comparison as direct as possible, the same type of potential was chosen, i.e. a slightly polydisperse Lennard-Jones potential $U_{ij}(r) = 4\epsilon\left((\sigma_{ij}/r)^{12} - (\sigma_{ij}/r)^{6}\right)$ where the σ_{ij} are taken uniformly distributed between 0.8σ and 1.2σ, corresponding to a polydispersity index of 0.12. This is expected to be enough to destabilise a polydisperse crystal [21], and indeed no sign of crystallisation or demixing was observed in our simulations. The interaction energy scale ϵ and the particle masses m will be taken to be strictly monodisperse. In the following, we will adopt the units appropriate for this Lennard-Jones systems, i.e. the mean diameter σ will be our unit of length (and generically described as the "particle size"), while time will be expressed in units of $\tau = \sqrt{m\sigma^2/\epsilon}$.

We studied various systems at constant density, $\rho = N/L^3 = 0.98$, which for our systems corresponds to a very low hydrostatic pressure at zero temperature ($|P| \approx 0.2$). The lateral size L of the system was varied between $L = 8$ and $L = 64$ (corresponding to $N = 500$ and $N = 256000$ particles).

Disordered configurations are prepared by melting at high temperature ($k_BT = 2\epsilon$) an initially FCC configuration during 10^5 Molecular Dynamics Steps (MDS) using constant temperature molecular dynamics and velocity-Verlet integrator with a step size of 0.001τ. After the system was equilibrated, we checked that no crystalline order remains, and we begin the production run using two types of minimisation. The first one, called the "fast" quench, uses a direct conjugate gradient minimisation until (according to numerical tolerance) the zero temperature equilibrium state is reached. This type of minimisation was implemented for all system sizes. The second one, which we called the "slow" quench, is implemented for systems containing up to $N = 62500$ particles, corresponding to a lateral size $L = 40$. The protocol used in this case consists in equilibrating the liquid configuration at intermediate temperature ($k_BT = 1\epsilon$) and then cooling this by stages ($k_BT = 5.10^{-1}\epsilon, 10^{-1}\epsilon, 5.10^{-2}\epsilon, 10^{-2}\epsilon, 5.10^{-3}\epsilon, 10^{-3}\epsilon$). At each stage, the system is "aged" (rather than equilibrated) during 10^5 MDS. Finally, the zero temperature state is reached using conjugate gradient minimisation from the last stage. Unless indicated otherwise, all the results discussed below refer to the fast quench procedure, which was carried out for all system sizes.

In order to obtain good quality statistics, this procedure was repeated between 1 and 10 times, depending on the system size. The results presented in the following are averages over these different realisations of our amorphous systems.

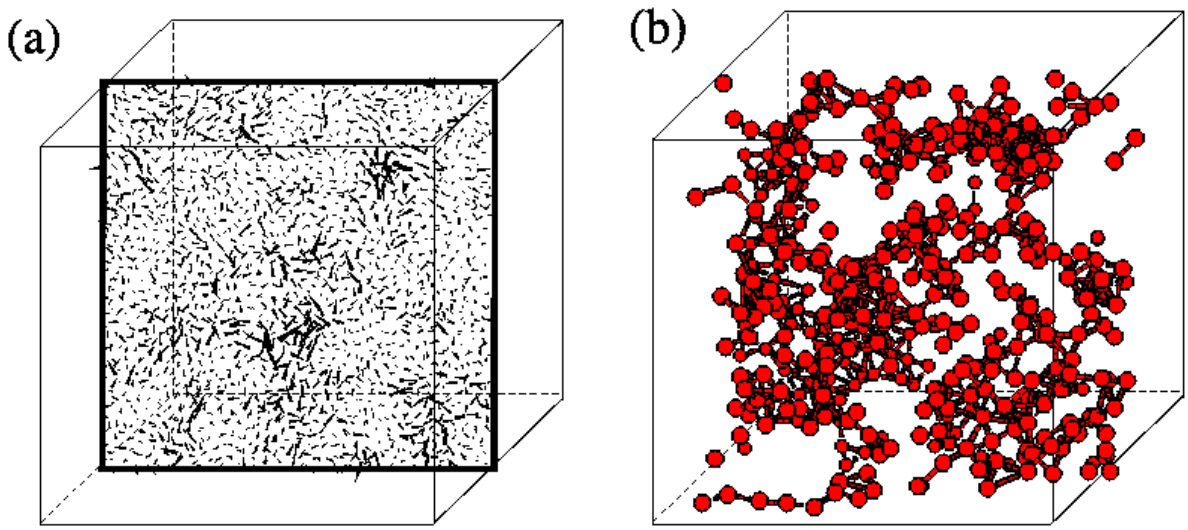

FIG. 1: Non-affine part of the linear and reversible displacement field $\underline{u}(\underline{r})$ for the imposed macroscopic uniaxial strain $\epsilon_{xx} = 10^{-7}$ for a system containing $N = 62500$ beads ($L = 40$): **(a)** projection on the $(x - z)$-plane for all particles close to the plane. The length of the arrow is proportional to the displacement. **(b)** all beads of the same configuration with the 10% strongest non-affine displacements. (The short lines indicate beads with direct mutual interactions.) This subset of beads is strongly spatially correlated on short distances, however, it is homogeneously distributed and isotropic on larger scales.

III. RESPONSE TO A MACROSCOPIC UNIAXIAL DEFORMATION

A. Computational procedure and non-affine displacement fields

In this section, we investigate the elastic behavior of zero temperature cubic samples, prepared as described above, submitted to an uniaxial traction. The procedure adopted is the following. First, a global deformation of strain $\epsilon_{xx} \ll 1$ is imposed on the sample by rescaling all the coordinates in an *affine* manner. Starting from this affinely deformed configuration, the system is relaxed to the nearest energy minimum, keeping the shape of the simulation box constant. As a result, a displacement of the particles relative to the affinely deformed state is observed. This defines the *non-affine* displacement field $\underline{u}(\underline{r})$.

A typical example for this field in the *linear elastic* response limit for a strain of $\epsilon_{xx} \approx 10^{-7}$) is presented in the first panel of Fig. 1. It displays a two dimensional projection of $\underline{u}(\underline{r})$ in a plane containing the elongation direction for a system of size $L = 40$. (Note that

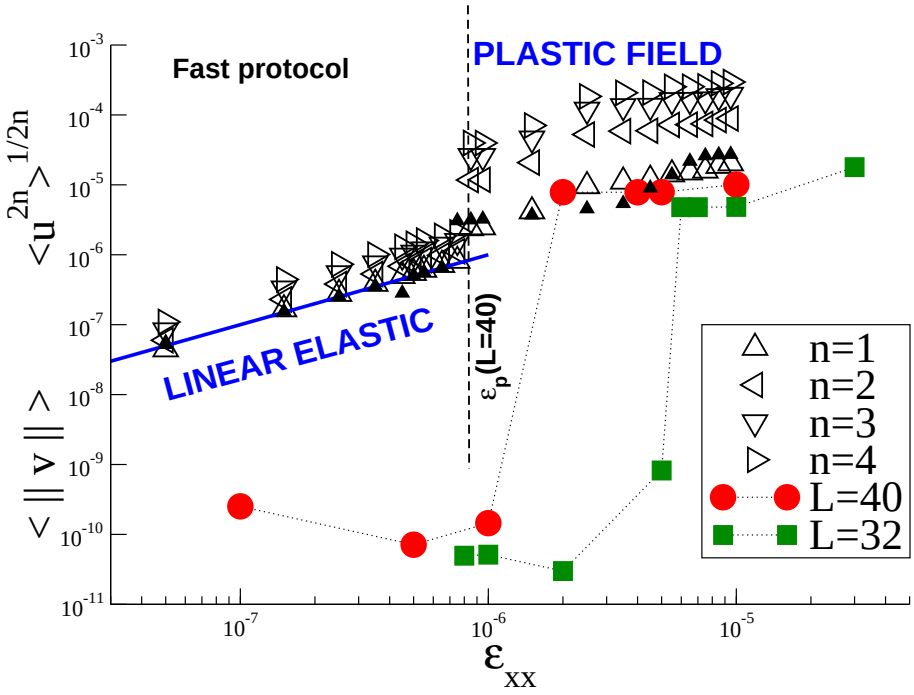

FIG. 2: Different moments of non-affine displacement field $\langle \underline{u}^{2n}\rangle^{1/2n}$ for $n = 1, 2, 3, 4$ as a function of the imposed strain ϵ_{xx} for systems of $L = 40$ obtained by means of the fast (open triangles) and the slow (full triangles) quench protocol. Both protocols show very similar results. The bold line on the left indicates the linear slope $\langle \underline{u}^{2n}\rangle^{1/2n} \propto \epsilon_{xx}$. The vertical dashed line marks the limit of elastic response $\epsilon_p(L) \approx 10^{-6}$ for $L = 40$. Also given is the residual plastic displacement field $\langle ||\underline{v}|| \rangle$ (obtained by reverse deformation back to the original macroscopic shape) for $L = 40$ and $L = 32$ (full symbols). Residual fields below 10^{-9} are due to numerical inaccuracies and the field can be considered as reversible. The sudden rise at ϵ_p for $L = 40$ corresponds nicely to the jump of the moments $\langle \underline{u}^{2n}\rangle^{1/2n}$. Note that the plasticity threshold ϵ_p depends strongly on the system size.

projections on different planes are similar.) Visual inspection of such snapshots suggests that non-affine fields are *strongly* correlated over short and intermediate distances. This impression is also confirmed by Fig. 1(b) where we focus on the 10% most mobile particles suggesting a connected cluster of these strong displacements spanning the simulation cell.

In Fig. 2 we present the first moments $\langle (\underline{u}(\epsilon_{xx}))^{2n}\rangle^{1/2n}$ of the non-affine displacement field of system of size $L = 40$ averaged over all particles of an ensemble. Both quench protocols are very similar. (Only one moment is given for the slow protocol for clarity.) For $\epsilon \ll \epsilon_p \approx 10^{-6}$ (vertical line) all moments are (up to prefactors of order one) identical which demonstrates an unique strain dependence for all beads. As one may also expect, a linear

strain dependence is found (bold line). At ϵ_p the moments increase suddenly and differ over more than an order of magnitude. This suggests an inhomogeneous strain dependence of the non-affine displacement field as will be discussed below (Fig. 3). We note finally that the threshold ϵ_p decreases strongly with the system size (not shown). Hence, linear response requires much smaller deformations for large L.

B. Plastic displacements and participation ratio

The elastic (reversible) character of the deformations was checked by carrying out the reverse transformation and measuring the residual displacement of the particles, $\underline{v}_i$, which corresponds to plastic deformation. The moment $\langle||v_i||\rangle_i$ of the residual field is indicated in Fig. 2. For $\epsilon_{xx} \ll \epsilon_p$ it is negligible and the deformation is, hence, elastic. Interestingly, elastic and linear elastic regimes coincide essentially as can be seen from the figure. For larger strains the residual displacements increase sharply over several orders of magnitude and coincide roughly with the $n = 1$ moment of the non-affine displacements. This shows that, for $\epsilon_{xx} > \epsilon_p$, the non-affine displacements are mainly due to plastic rearrangements.

In view of the potential relationship with plastic deformation, it is interesting to investigate in some detail the spatial features of the non-affine displacement field. Qualitatively, this can be achieved by representing, as shown in Fig. 1(b), the particles that have the 10% largest non-affine displacements. This picture shows that the non-affine field is rather delocalized, with the cluster formed by the most mobile particles spanning the entire simulation cell. A more quantitative view can be obtained by calculating the participation ratio for the non-affine displacement, defined by

$$P = \frac{1}{N} \frac{(\sum_i \underline{u}_i^2)^2}{\sum_i (\underline{u}_i^2)^2} \tag{1}$$

This participation ratio is shown in Fig. 3 for both quench protocols and $L = 40$. (A similar participation ratio may be calculated for the *residual* plastic field. However in this last case, the ratio at small ϵ is due to numerics and at high strain it is identical to the participation ratio of the non-affine field.) Obviously, for sufficiently small deformations the displacements must depend identically for *all* beads on the applied strain and P has to become constant. As anticipated in Fig. 2, the presented data shows that this coincides with the linear elastic regime where all moments of the non-affine field are similar and the residual plastic field

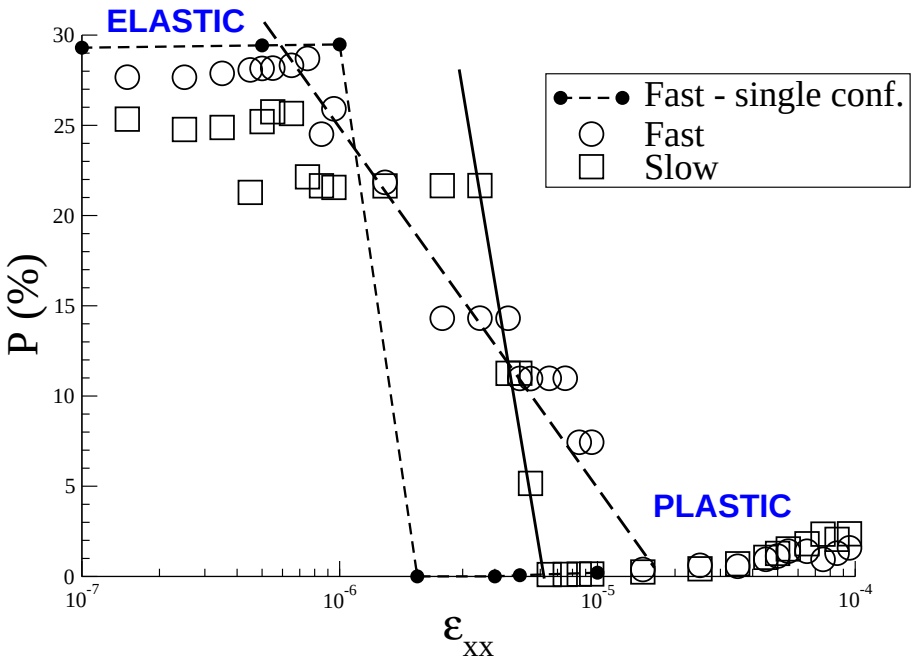

FIG. 3: Participation ratio of the non-affine displacement field in a 3D system containing 62500 particles ($L = 40$), as a function of the uniaxial strain ϵ_{xx}. Results for both fast and slow quench protocols averaged over eight and five configurations respectively. The given lines are guides to the eye. In the case of the fast protocol, a single configuration is also shown, for comparison with the averaged case.

can be neglected. [1] The central point is here that the plateau value of the participation ratio is large (about 25%) indicating that the elastic non-affine displacement involves a substantial fraction of the particles. When the deformation exceeds the plastic threshold ϵ_p, however, the participation ratio falls rapidly, indicating that a plastic deformation proceeds via well *localized* events. [2] This is the first main result of this work. The implication from this

[1] Note that the jumps in the plateau value at small strains (below 10^{-6}) in Fig. 3, specifically for the slow quench protocol, may be attributed to numerical inaccuracies due to the small displacement fields which have been compared.

[2] It should be stressed that the more gradual decay of the participation ratio, in the fast protocol case (Fig.3), is due to ensemble average. It describes essentially the probability that no jump has occurred for smaller ϵ values, and it is thus related to the distribution of the plastic thresholds ϵ_p from one configuration to the other. In the case of a single configuration, the decay of the participation ratio is more sudden, and can be compared with the averaged decay in the slow protocol case, where the distribution of ϵ_p is narrower. This is, in fact, the main difference observed between the two quench protocols: the plastic threshold ϵ_p is well defined in the slow quench protocol case, but it is largely distributed (over more that one decade) in the fast quench protocol case. Note however that we do not have, at this stage, a sufficient

difference in behavior is that the localized events occurring in plastic deformation cannot be directly inferred from the general *pattern* of non-affine displacements. This does not mean that plastic displacements and strong non-affine elastic displacements are completely uncorrelated.

In other words, energy barriers (which are relevant for plastic deformation) are not directly related to the local curvature of the energy minima [24]. Interestingly, the main influence of performing a slow quench seems to be that the plasticity limit is increased, meaning that the system has been brought to a slightly more stable configuration with higher energy barriers without, apparently, changing measurably the local curvature of the energy minima. In fact, properties such as the vibrational modes discussed below, are much less affected by the quench protocol.

In the reminder of this paper, we focus on the *linear* elastic response. We normalise the non-affine field by its second moment, i.e., $\underline{u}_i$ is replaced by $\underline{u}_i/\langle \underline{u}^2 \rangle^{1/2}$, in order to consider a strain independent reduced field.

C. Hydrodynamic limit: Lamé coefficients

We turn now to the calculation of the Lamé coefficients λ and μ, which characterize the elastic behavior of an isotropic medium in 3D [22]. Our results for these coefficients as a function of system size are shown in Fig. 4. This figure compares two different ways of obtaining the coefficients. λ_a and μ_a are obtained under the assumption that the non-affine contribution to the total displacement field of the particles is negligible. They are simply the Born estimates, that can be, in a system with pairwise interactions, computed from the reference configuration by carrying out a simple summation over all pairs of interacting particles (see for example ref. [6])

$$\lambda_a = \mu_a = \frac{1}{L^3} \sum_{i,j} \left(U''(r_{ij}) - \frac{1}{r_{ij}} U'(r_{ij}) \right) \frac{x_{ij}^2 y_{ij}^2}{r_{ij}^2} \tag{2}$$

where U is the interaction potential. The second estimate corresponds to the "true" value of the elastic coefficients, obtained by computing the actual stress in the sample *after* the relaxation that introduces the non-affine part of the displacement field. The averaged stress

number of configurations to compute more precisely this distribution.

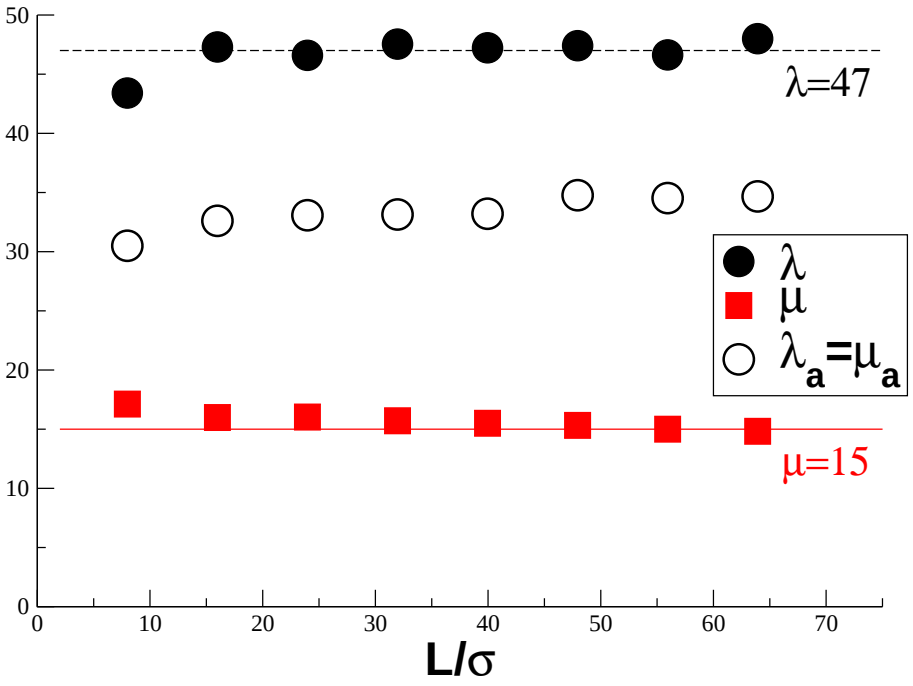

FIG. 4: Lamé coefficients λ (spheres) and μ (squares) *vs.* system size L. Full symbols correspond to the direct measurement using Hooke's law, open symbols are obtained from Eq. (2) which supposes *affine* deformations (Born term). The effect of system size is weak. For large boxes we get $\mu \approx 15$ and $\lambda \approx 47$. The coefficients relying on a negligible non-affine field differ by a factor as large as 2 from the true ones. Clearly, a calculation taking into account the non-affine character of the displacement is necessary for disordered systems.

is computed using the usual microscopic expression

$$\overline{\sigma}_{\alpha\beta} = \frac{1}{L^3} \sum_{i,j} (\underline{r}_{ij})_\alpha (\underline{F}_{ij})_\beta \tag{3}$$

where the Greek indices refer to cartesian coordinates, and $\underline{F}_{ij}$ is the force between particles i and j.

The Lamé coefficients are then obtained from the standard formulae $\overline{\sigma}_{xx} = (\lambda+2\mu)\epsilon_{xx}$ and $\overline{\sigma}_{yy} = \lambda\epsilon_{xx}$ for a deformation tensor which has only an ϵ_{xx} component (ϵ_{xx} is here the global deformation imposed on the sample). For larger systems, we obtain $\mu \approx 15$ and $\lambda \approx 47$. Hence, we find that the true values of λ and μ differ considerably from the Born estimates which indicates the importance of non-affine displacements in determining the stresses in the material. This contribution tends to lower the shear modulus μ, and to increase the coefficient λ. From the measured values of λ and μ we get a bulk compression modulus

$K = \lambda + 2\mu/d \approx 57$, a Young modulus $E = 8K\mu/(3K + \mu) \approx 37$ and a Poisson ratio $\nu = (3K - 2\mu)/2(3K + \mu) \approx 0.4$ [22]. Remarkably, the bulk modulus K would be correctly predicted by the Born calculation. This means that the non-affine part of the deformation does not contribute significantly to the increment in the *isotropic* pressure under compression or traction, but is mainly associated with shear deformations. (This point will be further elucidated below when we will discuss Fig. 7.) Such a situation would be natural in high pressure systems, in which the repulsive inverse power part of the potential dominates the interaction, and compression can be accommodated by an affine rescaling of all coordinates. It is, however, less expected in our low pressure systems.

D. Correlations in the non-affine displacement field

The preceding results call for a more thorough analysis of the correlations of the non-affine displacement field which apparently can not be neglected for macroscopic quantities and should therefore be even more relevant for finite wave length properties.

Following Ref. [1, 2], the non-affine correlation field can be analyzed by computing the correlation function $C(r) \equiv \langle \underline{u}(\underline{r}) \cdot \underline{u}(0) \rangle$. (The averages are taken over all pairs of monomers (i, j) being a distance r apart.) As can be seen in Fig. 5, a decay over a typical length of 23 particle sizes is observed (bold line), before the correlation function exhibits a *negative* tail (see inset). The 2D case (disks) is also included for comparison. Qualitatively similar behavior is found. The anti-correlation can be associated visually in 2D with the solenoidal character of the non-affine field [1, 2]. The organisation of the non-affine deformation in "vortices" is less obvious in 3D (see inset) as manifested by the about seven times weaker amplitude of the negative tail. However, this description can be compared with the direct visualization of Fig. 1, where the intricate structure of the vortices is shown. See also Fig. 7 below.

That the displacement field is indeed correlated over a size $\xi \gg \sigma$ is further elucidated in Fig. 6. Here we consider the systematic coarse-graining of the displacement field

$$\underline{U}_j(b) \equiv \frac{1}{N_j} \sum_{i \in V_j} \underline{u}(\underline{r}_i) \tag{4}$$

of all N_j beads contained within the cubic volume element V_j of linear size b. In the figure, we have plotted the (normalized) correlation function $B(b) \equiv (\langle \underline{U}_j(b)^2 \rangle_j / \langle \underline{u}^2 \rangle)^{1/2}$ versus the

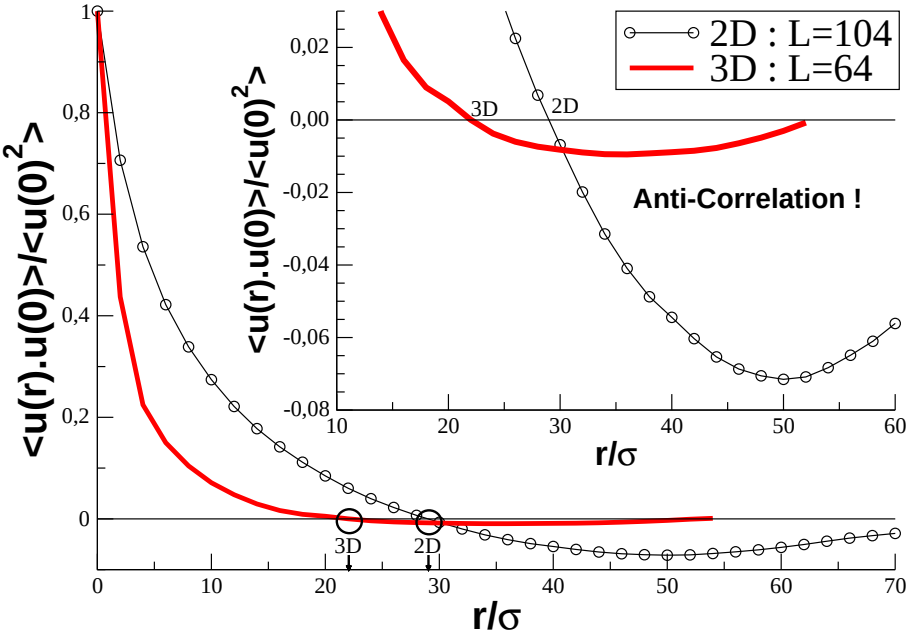

FIG. 5: Correlation function $C(r)$ of the non-affine deformation field as a function of the distance between pairs of beads r. The correlation function is averaged over all possible pairs. The full line corresponds to a 3D sample containing 256000 particles ($L = 64$). Note that the "fast" quench protocol and the "slow" quench protocol (not shown here) give the same curve. Data from [1] for a 2D system of linear size $L = 104$ is shown for comparison (line with open dots). In the 2D case, results are averaged over 30 configurations. The data are plotted in linear scale. Inset: Enlargement of the anti-correlation regime. Note the *negative* – although weak – correlation of the 3D correlation function for $r > 23\sigma$.

size of the coarse-graining volume element b (normalized by L). Two and three dimensional systems are again compared. In both cases we find an *exponential* decay which is well fitted by the characteristic scales $\xi \approx 23$ for 3D and $\xi \approx 42$ for 2D. Apparently, ξ is similar to the distance where $C(r)$ becomes anti-correlated. Note that the total non-affine displacement field of the box must vanish – since the center of mass of the system is fixed– and therefore $B(b) \to 0$ for $b/L \to 1$. This sum rule explains the curvature in the data and the sharp cut-off on the right hand side of the figure. The nice agreement of both estimations of ξ demonstrated in the Figs. 5 and 6 and the similar behavior in both dimensions is the second central result of this work.

More systematically, the displacement field can be investigated in Fourier space $\underline{U}(\underline{k}) \equiv \sum_{i=1}^{N} \underline{u}(\underline{r}_i) \exp(i\underline{k} \cdot \underline{r}_i)$. Apart the normalisation factor $1/N_j$, this is close to the volume

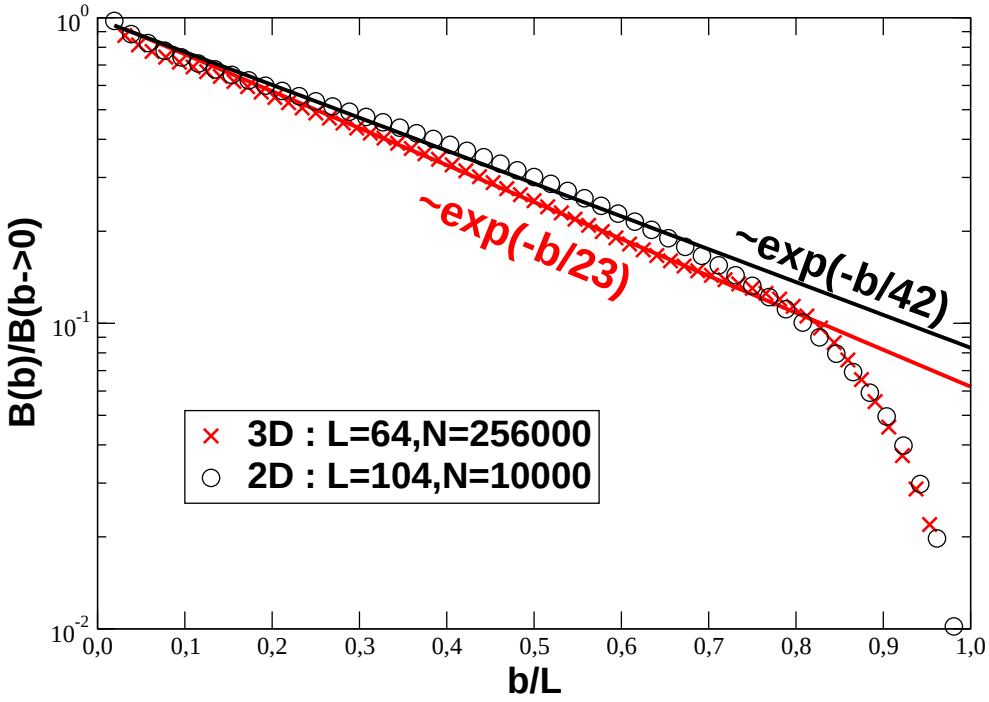

FIG. 6: The (normalized) magnitude $B(b)$ of the non-affine field averaged over a volume element of lateral size b is traced as a function of b/L. The plot confirms that the correlations decay with a characteristic length $\xi = 23$ for 3D and $\xi = 42$ for 2D (spheres, for 10 configurations) respectively.

element coarse-graining method, Eq. (4). As usual, the fluctuations can be directly computed from $S(k) \equiv \frac{1}{N}\langle||\underline{U}(\underline{k})||^2\rangle$ where the average is taken over all wave vectors with $k = ||\underline{k}||$. Our results for $S(k)$ are not presented since we prefer to discuss below in Fig. 7 the longitudinal and transverse contributions, $S_L(k)$ and $S_T(k)$. Note also, that $S(k)$ is related to the real space coarse-graining correlation function $B(b)$ of linear size $b = 2\pi/k$ given in Fig. 6.[3] Interestingly, it can be readily shown that

$$S(k) = \frac{1}{N}\sum_{i,j}\exp(i\underline{k}\cdot(\underline{r}_i - \underline{r}_j)\langle\underline{u}(\underline{r}_i)\underline{u}(\underline{r}_j)\rangle = \langle u^2\rangle + \int d\underline{r}\exp(i\underline{k}\cdot\underline{r})C(r)\rho g(r) \qquad (5)$$

[3] The wave vector $\underline{k}$ must be chosen commensurate with the periodic simulation box. For this reason fewer values of the wave length $\lambda = 2\pi/||\underline{k}|| = L/\sqrt{(n^2+m^2+l^2)}$ (n, m and l being integers) can be computed. This is the principle disadvantage of the Fourier transformation of the non-affine field for computational studies in 3D – where the system size is necessarily rather limited – compared to the real space coarse-graining method which allows also a continuous variation of the box length b. Moreover, it is easy to show that $B^2(b)$ is the average over a volume b^d of the correlation function $C(r)$ whose Fourier transform is related to $S(k)$. Thus a clearly shown size dependence of $B(b)$ can be masked in the power law decay of $S(k)$ (at large k).

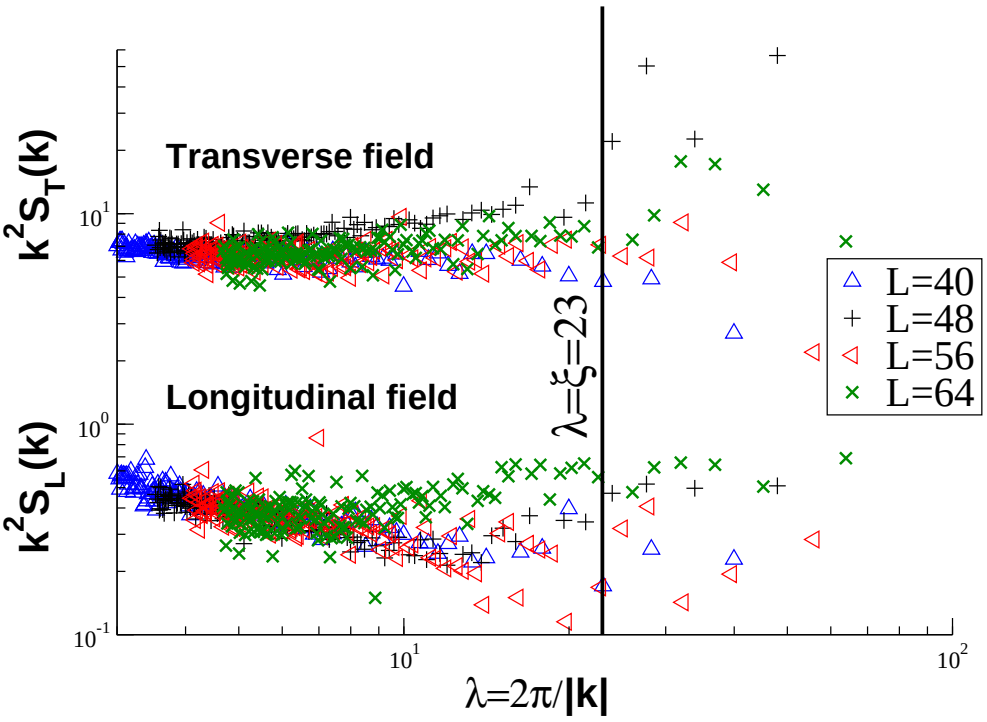

FIG. 7: The squared amplitudes of the Fourier transforms k^2S_L and k^2S_T for the div (lower data) and curl (upper data) of the non-affine deformation field (see Eq. (7)) plotted as functions of the wave length $\lambda = 2\pi/||\underline{k}||$. Different system sizes, as indicated in the figure, have been included to demonstrate that S_L and S_T are essentially system size independent for small λ. Note that the statistics deteriorates for large λ.

with $C(r)$ being the displacement correlation function discussed in Fig. 5 and $g(r)$ the standard pair distribution function. Since $g(r)$ becomes rapidly constant it follows that $S(k)$ corresponds essentially to the Fourier transform of $C(r)$. This demonstrates that (very roughly) $C(r)$ and $B(b)$ (shown in Fig. 5 and 6 respectively) are related by Fourier transformations and explains why similar characteristic sizes $\xi \gg \sigma$ have been obtained.

We demonstrate now that the non-affine displacement field in 3D is indeed of predominantly *solenoidal* nature. This has been anticipated by our previous studies on 2D systems [1] and by the values of the elastic moduli μ and K discussed in Sec. III C. The transverse and longitudinal contributions to the displacement field can be numerically obtained by computing

$$\underline{T}(\underline{k}) \equiv -\frac{1}{k^2}\underline{k} \wedge (\underline{k} \wedge \underline{U}(\underline{k})) \ , \ \underline{L}(\underline{k}) \equiv \frac{1}{k^2}\underline{k}\,(\underline{k} \cdot \underline{U}(\underline{k})) \tag{6}$$

Obviously, $\underline{U} = \underline{T} + \underline{L}$, $\underline{k} \cdot \underline{U} = \underline{k} \cdot \underline{L}$, $\underline{k} \wedge \underline{U} = \underline{k} \wedge \underline{T}$ and $\underline{k} \cdot \underline{T} = \underline{k} \wedge \underline{L} = 0$. The norms of

these quantities, for instance

$$k^2 S_T(k) \equiv \frac{k^2}{N} \langle ||\underline{T}(\underline{k})||^2 \rangle = \frac{1}{N} < || \sum_i \underline{k} \wedge \underline{u}(\underline{r}_i) \exp(i\underline{k} \cdot \underline{r}_i)||^2 > \tag{7}$$

and similarly for the longitudinal part $k^2 S_L(k)$, are the Fourier transforms of $\underline{\nabla} \wedge \underline{u}$ and $\underline{\nabla u}$. They are plotted in Fig. 7 as functions of $\lambda = 2\pi/k$. We find that the longitudinal contribution (data points at the bottom) is about 10 times smaller than the transverse one. Note that all data points of different system sizes collapse well for wavelengths corresponding to the non-affine displacement regime, $\lambda < \xi$. We find that $k^2 S_T(k)$ is more or less constant while $k^2 S_L(k)$ decreases weakly. Since $\underline{T}$ and $\underline{L}$ are orthogonal this yields $S(k) = S_T(k) + S_L(k) \approx S_T(k)$ and, hence, the algebraic relation $S(k) \propto 1/k^2$ for large k. [4] Unfortunately, for larger λ the statistics deteriorates due to the smaller number of wave vectors which can be considered. Our data may suggest that $S_T(k)$ increases for $\lambda > \xi$, however, new data with larger boxes and with better statistics is warranted to confirm this.

[4] see previous footnote.

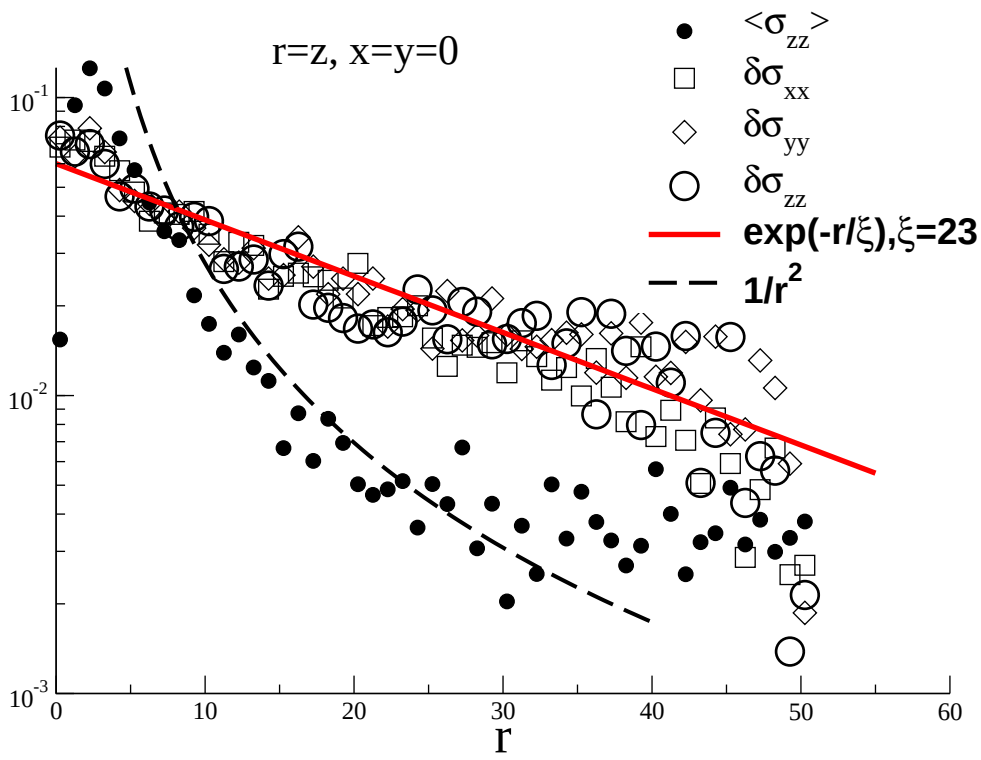

FIG. 8: Comparison of the incremental stress fluctuations $\delta\sigma_{\alpha\beta} \equiv (< \sigma_{\alpha\beta}^2 > - < \sigma_{\alpha\beta} >^2)^{1/2}$ with the mean vertical component of normal stress $< \sigma_{zz} >$ for the ensemble average discussed in text, measured along the vertical line ($x = y = 0$). The mean stress decreases essentially as $1/r^2$, as expected (without logarithmic corrections) in 3D for positions far from the source and the fixed walls. (Note that $< \sigma_{zz} >$ has to decrease less rapidly close to the walls, $r \approx L/2$.) In contrast, the fluctuations decay exponentially over the whole available system. The characteristic length scale is similar to the size $\xi \approx 23\sigma$ of the correlated non-affine displacements.

IV. SELF-AVERAGING OF THE RESPONSE TO A POINT FORCE

In 2D, we showed previously [3] that the deviations from continuum elasticity at small scales could be revealed by studying the response of the system to a localised force. The same effect is illustrated for 3D in Fig. 8. This plot is obtained as follows. A small force is applied to the particles contained in a small region of space (sphere of diameter 4). The force is applied in the z direction, and its magnitude is chosen small enough to remain in the (linear) elastic region ($F_z = 10$). In order to maintain global force balance, the system has periodic boundary conditions in the x and y directions, but is immobilised by two fixed walls in the z direction. The dimensions of the simulation cell, which contains $N = 165000$

particles, are $L_z \simeq 105$ in the z direction, $L_x = L_y \simeq 40$ in lateral directions. The stress tensor is then measured within the sample using the standard Kirkwood definition [13] calculated in small rectangular boxes of fixed size $(3, 3, 5)$ centered in (x, y, z). Those boxes are displaced in all the material by unit steps of one in the three directions. For each step the six components of the stress tensor are calculated and averaged on a statistical ensemble of 200 configurations. Such an ensemble is obtained by taking 10 independent configurations, and for each configuration by changing the position of the point source within the sample reindexing the configuration in such a way that the origin of the source still is placed in the midplane, equally distant from the two fixed walls. In the absence of the external force, the local stresses in amorphous systems are usually nonzero ("quenched stresses"). The relevant quantity that defines the response to an external force are therefore the incremental, rather than total, local stress tensor. Once such a calculation done, the quantity of interest is the fluctuations of the stress tensor in the statistical ensemble [3].

In Fig. 8, both the average value and the fluctuations of the stress tensor are shown. The average response is compared to the prediction of continuum elasticity, which appears to be perfectly obeyed *on average* even very close to the source. This average response exhibits the $1/r^2$ decay characteristic of the Green function of classical elasticity in 3D. However, up to length scales of 50 the fluctuations are considerably larger than the average value of the stress. The fluctuations, on the other hand decay *exponentially* away from the source, with a characteristic length 23 – the same value as obtained from the correlation functions discussed in the previous section. In fact, the *relative* stress fluctuations, for instance $\delta\sigma_{zz}/\langle\sigma_{zz}\rangle$, scale like $\exp(-r/\xi)r^2$ and show non-monotoneous behaviour (not shown). They *increase* first up to 2ξ (due to the decreasing mean stress), but decrease ultimately exponentially. With other words, *self-averaging* (within every configuration) of the noisy signal occurs on distances set by ξ which we call, hence, the *self-averaging length.* [5] Unfortunately, our simulation boxes are yet too small to illustrate more clearly the exponential decay of the relative noise for $r \gg 2\xi \approx 50$.

[5] Absolutely similar behaviour has also been found in 2D systems [3]. There the relative fluctuations scale like $\exp(-r/\xi)r$, i.e. exponential screening sets in for distances $r \gg \xi$. Since ξ is about twice larger in 2D it turns out that about the *same* linear distance is required in both dimensions for self-averaging to become effective. This suggests that if different dimensions d are compared one should rather use the notion "self-averaging length" for $(d-1)\xi$.

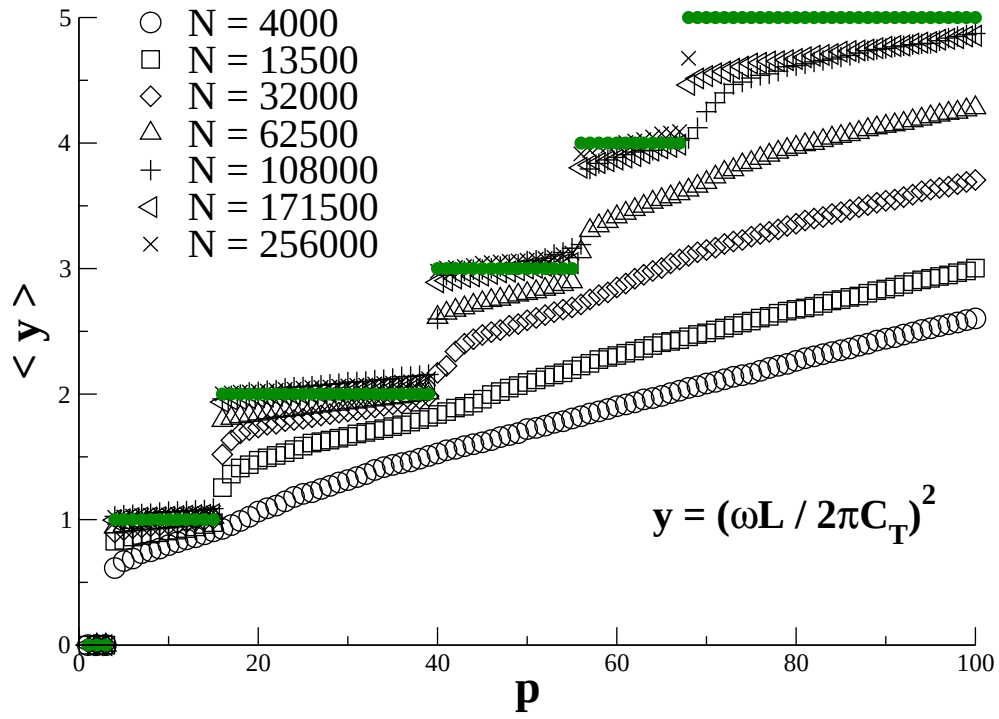

FIG. 9: Eigenfrequencies ω of the first 100 modes as a function of mode number p. The frequencies are rescaled using the system size and the sound velocity (obtained from the Lamé coefficient in Fig. 4). The horizontal lines correspond to the results expected from macroscopic elasticity. Frequencies of small systems are systematically too low. Besides the obvious Goldstone modes ($p = 1, 2, 3$), all frequencies are finite.

V. LOW FREQUENCY EQUILIBRIUM VIBRATION MODES

We turn now to the determination of low frequency vibration modes. These were determined from a direct diagonalization of the dynamical matrix, using a modified version of the PARPACK package [23]. For a periodic cubic system described by classical elasticity, the structure of the low frequency end of the spectrum is well known. Each mode is characterised by a wave vector $\underline{k} = \frac{2\pi}{L}(l, m, n)$. Transverse (resp. longitudinal) have frequencies $\omega = c_T k$ (resp. $\omega = c_L k$), where the sound velocity is given by $c_T = \sqrt{\mu/\rho} \approx 4.2$ (resp. $c_L = \sqrt{(\lambda + 2\mu)/\rho} \approx 8.9$). As a result, the modes should have well defined degeneracies. For example, the lowest lying mode $(\pm 1, 0, 0)$ should have 12 fold degeneracy, corresponding to the two transverse polarisations for the 6 wave vectors of length $2\pi/L$. The second frequency has degeneracy 24, and so on. In our previous analysis of 2D systems [1], we found that this

degeneracy of the low frequency modes was lifted for small systems sizes. A scaling analysis of the modes allowed to establish in a different manner the length scale ξ, above which the medium can be considered as elastically homogeneous.

Our results for the low frequency modes of three dimensional systems are shown in Fig. 9. Plotting the rescaled and averaged frequencies $\langle y \rangle = \langle (\omega L/2\pi c_T)^2 \rangle$ as a function of mode number p, [6] it is clear that the degeneracies and the associated step-like behavior begin to show up only for large systems, containing at least 32000 particles (lateral size 32). For the largest systems however (lateral size 64) the discreteness of the low frequency spectrum is well apparent, typically up to the 4th eigenfrequencies. In view of the large value of c_L compared to c_T ($c_L \simeq 2.1 c_T$ in our system) we have concentrated on the analysis of transverse modes. Longitudinal modes enter only at higher frequencies, and are mixed with shorter wave length transverse modes, making their contribution more difficult to identify. If we take as a criterion the existence of a gap separating the first 12 eigenfrequencies from the rest of the spectrum, it appears that the minimum size for applying continuum elasticity is comprised between $L = 16$ and $L = 32$ particle sizes.

This analysis can be refined using a scaling plot of the mode frequencies as a function of the "theoretical" wave length, or more precisely the wave length of the elastic wave that would appear in the spectrum with this mode number according to elastic theory. Fig. 10 is constructed by averaging, for each size, the frequencies that correspond to the first elastic mode in elastic theory (e.g. the first 12 frequencies are averaged to obtain the lowest frequency point, the next 24 for the second point, and so on). The resulting frequency, divided by the value expected from elastic theory, is plotted as a function of wave length. Note that all data points collapse on the same master curve irrespective of the box size L. The plot shows that when the wave length is lower than the self-averaging length, deviations from elastic theory become significant, whatever the size of the system. This estimate for the size of elastic inhomogeneity is therefore in fair agreement with those obtained in two previous sections from the analysis of the linear response to an external load.

[6] The rescaling eliminates trivial dependencies on system size and sound velocities which are anyway expected from continuum theory. The rescaled frequencies are averaged over the ensemble of available configurations. Note that differences between the eigenfrequencies of different configurations of the ensemble are weak, however, even for small system sizes.

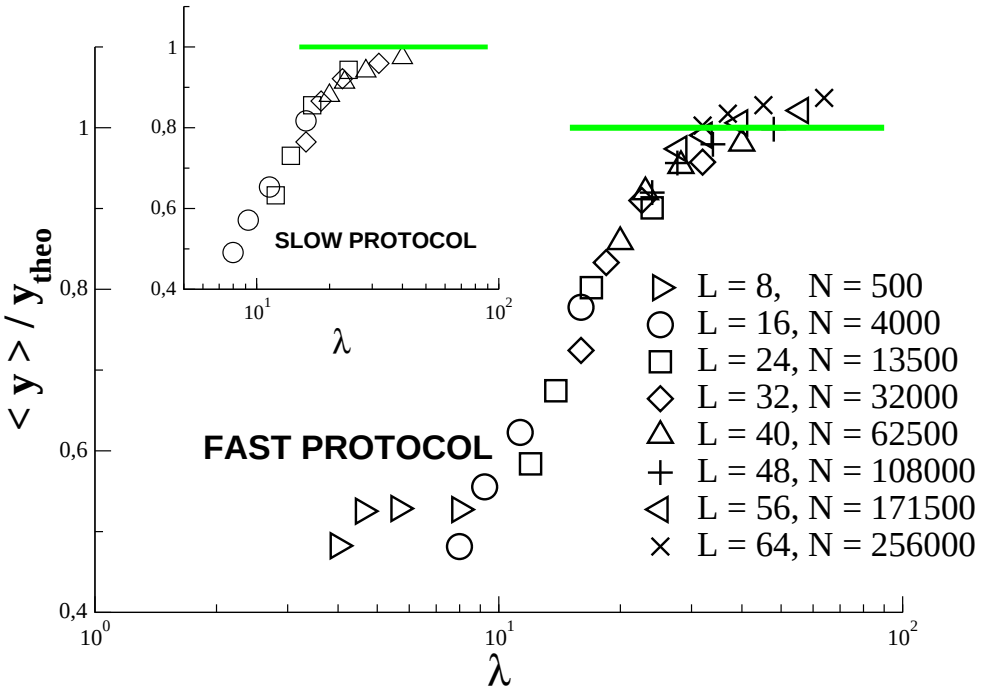

FIG. 10: Eigenfrequencies corresponding to the first four levels predicted by continuum elasticity, plotted as a function of the corresponding wavelength $\lambda = 2\pi/ \parallel \underline{k} \parallel$. The eigenfrequencies ω have been rescaled by their continuum theory values. This yields a perfect collapse of all data points. See main text for details. The crossover to continuum behavior (indicated by the horizontal line) takes place, as expected, at the self-averaging length $\lambda \simeq \xi$. The frequencies decrease systematically with smaller λ. Inset: The same plot for the slow quench protocol shows barely distinguishable behavior (same symbols as in the main plot).

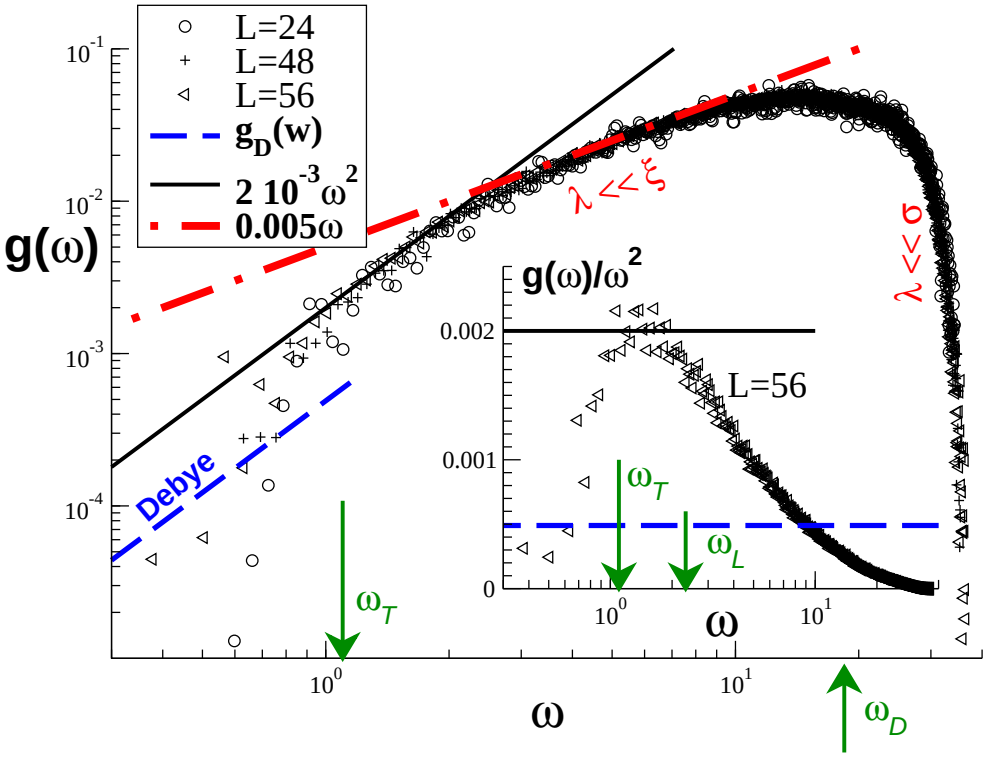

FIG. 11: Density of states $g(\omega)$ for 3D amorphous systems of different system sizes L. The lines indicate three power law slopes, the dashed one being the Debye prediction $g_D(\omega)$ calculated from the known sound velocities. The dashed-dotted linear relation corresponds to the non-affine displacement field regime ($\lambda \ll \xi$). Also given are the characteristic frequencies $\omega_{L,T} = c_{L,T} 2\pi/\xi$ associated with the self-averaging length ξ and the Debye frequency $\omega_D \approx 18.3$. Larger frequencies correspond, in fact, to vibrations on very small scales, $\lambda \ll \sigma$. Inset: $g(\omega)/\omega^2$ *vs.* ω for $L = 56$ (same symbols as main figure). Note that ω_T and ω_L describe correctly the position and width of the boson peak.

VI. DENSITY OF VIBRATIONAL STATES

The (normalized) density of vibrational states (DOS) of a 3D solid may be defined by $g(\omega) = \frac{1}{3N} \sum_{p=1}^{3N} \delta(\omega - \omega_p)$ with ω_p being the harmonic eigenfrequency corresponding to the mode number p. Hence, for small systems (of order of 10^3 beads) one can compute the complete DOS from the eigenfrequencies extracted by exact diagonalization of the dynamical matrix, just as we have done in the previous section. Obviously, for systems containing about 10^5 particles the number of modes one may compute is rather limited. From the 100 modes we have presented in Fig. 9 one estimates roughly $\omega_p^2 \propto p^\alpha$ with $\alpha \approx 1$. Hence, the DOS

increases approximately linearly, $g(\omega) \propto \omega^{2/\alpha-1} \approx \omega$, for small ω.

Following standard procedures [19], we have instead obtained $g(\omega)$ by Fourier transformation of the velocity auto-correlation $\langle \underline{v}(t) \cdot \underline{v}(0) \rangle$. In contrast to the previous sections, we consider here configurations at finite, yet very low temperatures T. For the data presented in Fig. 11 we have used $T = 10^{-4}$ which is three orders of magnitudes below the glass transition of our systems. We start with quenched configurations at $T = 0$ which we subject to a Maxwell velocity distribution. Following a thermalization phase of $\delta t = 10^3$ the velocity correlation function is sampled over $\delta t = 100$. Different temperatures have been checked and we have verified that the DOS becomes temperature independent at low T (not shown). As can be seen from the Fig. 11, our results become rapidly system size independent for sufficiently large frequencies $\omega \gg c_{T,L} 2\pi/L$. We remember that only ω values corresponding to wave vectors $\underline{k}$ compatible with the box size are physically acceptable in the continuum limit. The corresponding finite size effects at low frequencies can be seen on the left hand side of the figure.

In linear coordinates, $g(\omega)$ is roughly symmetric around its maximum at $\omega \approx 14.3$ and may be very crudely described as linear for small ω in agreement with the estimate from Fig. 9 described above and the dashed-dotted line indicated in the main panel of Fig. 11. Note that the maximum is slightly smaller than the Debye frequency $\omega_D = (18\rho\pi^2/(1/c_L^3 + 2/c_T^3))^{1/3} \approx 18.3$ for our systems. (The Debye frequency is in turn smaller than the frequency $c_T 2\pi/\sigma \approx 26.4$ associated with a wave length of monomer size.) The log-log plot presented in the main figure shows various frequency regimes. For very small frequencies our data is roughly in agreement with the Debye continuum prediction $g_D(\omega) = 3\omega^2/\omega_D^3$ (dashed line). The DOS increases than more rapidly with frequency up to $\omega_T = c_T 2\pi/\xi \approx 1.1$ – corresponding to a wave vector given by the self-averaging length – where $g(\omega)$ has power law slope of exponent 2 (bold line). This can be more clearly seen in the inset featuring the enigmatic Boson peak. Apparently, the width of this peak is well described by ω_T and the frequency $\omega_L \approx 2.3$ for the corresponding longitudinal wave. Hence, the boson-peak is fixed by the self-averaging length and marks the crossover between the continuum elastic behavior (dashed line) and the non-affine displacement field regime, where $g(\omega) \propto \omega$ (dashed-dotted line), at larger ω and smaller wave length λ. Since continuum theory overestimates the frequencies for $\lambda \ll \xi$ (see also Fig. 10) this implies an excess of modes at smaller frequencies. Apparently, these modes are shifted to the edge of the non-affine regime. The boson-peak is merely a consequence of

the inapplicability of the continuum theory at $\lambda \ll \xi \approx 23$.

VII. CONCLUSION

We have investigated the approach of the continuum limit for elastic properties of 3D amorphous systems and compared our computational results with our previous work on similar 2D systems. The results are extremely similar in both cases, and can be summarized as follows. The elastic constants estimated using the Born formulae are not accurate even at zero temperature, therefore revealing the importance of the non-affine component of the deformation field. This non-affine deformation field, which affects mostly the shear response (as compared to compressibility) is correlated over intermediate distances, of the order of 23 interatomic distances in our case. This correlation length is significantly smaller than in 2D, in agreement with the findings of Rossi *et al* [17], but implies that rather large samples should be used to discuss elastic or vibrational properties of 3D systems as well. By considering the Fourier transformation of solenoidal and longitudinal part of the non-affine field we have demonstrated (Fig. 7) that the 3D non-affine field is mostly rotational in nature, in agreement with the visual impression of snapshots. The response to a delta force perturbation allowed us to measure the self-averaging of the noisy response within a configuration. The stress fluctuations decay exponentially with distance from the source with a characteristic length given by the correlation length ξ of the non-affine field which suggests to us the notion "self-averaging length".

Vibrational modes are obviously strongly affected by the existence of elastic heterogeneities, and cannot be predicted using elastic theory if their wave length is too small. From our scaling analysis (Fig. 10) it appears that the frequencies are *smaller* than expected from continuum theory, therefore implying an excess of modes in the low frequency region compared to the Debye prediction. This excess has been analyzed in Fig. 11 showing the density of vibrational states and demonstrating that the "boson peak" is located at the edge of the non-affine displacement field. That both position and width of the peak are given by the self-averaging length ξ is the central novel result of this work which has not been previously established for 2D systems.

The focus of this work has been primarily on the *linear elastic* behavior of amorphous solids. Our preliminary study of larger (uniaxial) deformations that go beyond the elastic

limit indicates that plastic events are rather localized individual events characterized by a very low participation ratio. In the recent work [15] de Pablo and coworkers pointed out the possibility of *regions of negative shear modulus* in quenched amorphous systems - such regions being stabilized by the "normal" material in which they are embedded. The typical size of these regions is much smaller than the size for elastic inhomogeneities discussed in this work, implying they are more likely to be linked to elementary rearrangements taking place at the onset of plastic deformation, which usually imply small numbers of particles [6, 7, 8, 9, 24], or even localization along a shear band [10, 11]. Such a difference in elastic and plastic deformations was also observed for 2D systems in Ref. [6].

The general picture that emerges is therefore that of a hierarchy of length scales. Disorder at the level of 2-3 atomic distances can be interpreted as implying the existence of regions with negative moduli, which will give rise to plastic yield. On a larger scale, this disorder gives rise to strong non-affine displacement fields in elementary deformations. Finally, convergence to standard continuum properties is obtained over length scales larger than the self-averaging length. In our analysis, carried out for a typical liquid state density and at zero-temperature, ξ is found to be large, but finite. In analogy with what is found in 2D, we expect it to decrease with increasing density, and possibly to diverge as the density is lowered and the system loses mechanical stability, as suggested in Ref. [16].

Acknowledgments

During the course of this work, we had valuable discussions with A. Lemaître, C. Maloney, J. de Pablo, B. Schnell and D. Vandembroucq. Computational support by IDRIS/France is acknowledged. F.L. was supported by the Emergence 2002 Program of the Conseil Regional Rhônes-Alpes (France).

[1] J.P. Wittmer, A. Tanguy, J.-L. Barrat, and L. Lewis, Europhys. Lett. **57**, 423 (2002)

[2] A. Tanguy, J.P. Wittmer, F. Leonforte, and J.-L. Barrat, Phys. Rev. B **66**, 174205 (2002).

[3] F. Leonforte, A. Tanguy, J. P. Wittmer, and J.-L. Barrat Phys. Rev. B **70**, 014203 (2004)

[4] E. Duval, A. Mermet, Phys. Rev. B **58**, 8159 (1998)

[5] V.A. Luchnikov, N.N. Medvedev, Y.I. Naberukhin and V.N. Novikov, Phys.Rev. B **51**, 15569 (1995).

[6] C. Maloney and A. Lemaître, Phys. Rev. Lett. **93**, 016001 (2004); Phys. Rev. Lett. **93**, 195501 (2004) ; A. Lemaître, C. Maloney, preprint condmat/0410592, to appear in J. Stat. Phys.

[7] M. Falk, J. Langer, Phys. Rev. E, **57**, 7192 (1998); Phys. Rev. B, **60**, 7062 (1999).

[8] J.Y. Cavaillé, J. Perez and G.P. Johari, Phys. Rev. B **39**, 2411 (1989).

[9] A. Kabla and G. Debrégeas, Phys. Rev. Lett. **90**, 258303-1 (2003).

[10] J.C. Baret, D. Vandembroucq and S. Roux, Phys. Rev. Lett. **89**, 195506 (2002).

[11] G. Picard, A. Ajdari, F. Lequeux and L. Bocquet, Phys. Rev. E **71**, 010501(R) (2005).

[12] M.D. Ediger, Ann. Rev. Phys. Chem. **51**, 99 (2000).

[13] I. Goldhirsch and C. Goldenberg, Eur. Phys. J. E **9**, 245 (2002).

[14] F. Leonforte *et al*, in preparation.

[15] K. Yoshimoto, T.S. Jain, K. van Workum, P.F. Nealey, J.J. de Pablo, Phys. Rev. Lett. **93**, 175501 (2004).

[16] L.E. Silbert, A.J. Liu, S.R. Nagel, preprint condmat/0501616. M. Wyart, S.R. Nagel and T.A. Witten, preprint condmat/0409687.

[17] B. Rossi, G. Viliani, E. Duval, L. Angelani, W. Garber, preprint 2005.

[18] V.A. Luchnikov, N.M. Medvedev, Yu.I. Naberukhin, and H.R. Schober, Phys. Rev. B **62**, 3181 (2000); H.R. Schober and C. Oligschleger, ibid. **53**, 11 469 (1996); H.R. Schober and B.B. Laird, ibid. **44**, 6746 (1991).

[19] S. V. Meshkov, Phys. Rev. B **55**, 12113 (1997).

[20] P.B. Allen, W. Garber, L. Angelani, condmat/0307435 (2003).

[21] J-L. Barrat, J-P. Hansen, J. de Physique **47**, 1547 (1987) P.N. Pusey, J. de Physique, **48**, 709 (1987)

[22] L.D. Landau and E.M. Lifshitz, *Theory of Elasticity* (Butterworth-Heinemann, London, 1995).

[23] Free software developed by R. Lehoucq, K. Maschhoff, D. Sorensen and C. Yang, Rice university. See http://www.caam.rice.edu/software/ARPACK/.

[24] D. Malandro, D. J. Lacks, J. Chem. Phys. **110**, 4593 (1999).